Effect of chemical heat release in a temporally evolving mixing layer

By F. J. Higuera[1] AND R. D. Moser[2]

Two-dimensional numerical simulations of a temporally evolving mixing layer with an exothermic infinitely fast diffusion flame between two unmixed reactants have been carried out in the limit of zero Mach number to study the effect of the heat release on the early stages of the evolution of the flow. Attention has been directed to relatively large values of the oxidizer-to-fuel mass stoichiometric ratio typical of hydrocarbon flames, and initial vorticity distributions thicker than the temperature and species distributions have been chosen to mimic the situation at the outlet of a jet. The results show that, during the stages of the evolution covered by the present simulations, enhancement of combustion occurs by local stretching of the flame without much augmentation of its area. The rate of product generation depends strongly on the initial conditions, which suggests the possibility of controlling the combustion by acting on the flow. Rollup and vortex amalgamation still occur in these reacting flows but are very much affected by the production of new vorticity by baroclinic torques. These torques lead to counter rotating vortex pairs around the flame and, more importantly, in thin layers of light fluid that leave the vicinity of the flame when the Kelvin-Helmholtz instability begins to develop. Propelled by the vortex pairs, these layers wind around, split on reaching high pressure regions, and originate new vortex pairs in a process that ends up building large-scale vortices with a vorticity distribution more complex than for a constant density fluid.

1. Introduction

Combustion typically involves large amounts of energy release that very often result in strong couplings of the molecular transport and chemical reactions with the motion of the gas where such processes occur. A fast chemical reaction between two initially unmixed reactants in a mixing layer is a prototype of many practical situations. In this case reaction occurs in a very thin flame controlled by the diffusion of the reactants from the carrying streams. Furthermore, the diffusion fluxes reaching the flame depend on the nature of the flow through the action of large-scale mixing and by the stretching and wrinkling that the flow imposes on the flame. Conversely, the flow may be very much affected by the gas expansion and baroclinic torques due to the chemical heat release. The coupled problem rapidly becomes very complicated and much work is required to analyze the elements of the coupling separately.

1 E.T.S. Ingenieros Aeronáuticos, Pza. Cardenal Cisneros 3, 28040 Madrid, Spain
2 NASA Ames Research Center

Experimental investigations of gas-phase reacting shear flows under conditions of low heat release, with no apparent coupling between heat release and the fluid mechanics, have been conducted by Mungal & Dimotakis (1984), Mungal, Hermanson & Dimotakis (1985) and Mungal & Frieler (1988) using the hydrogen-fluorine reaction, and by Masutani & Bowman (1986) using the nitric oxide-ozone reaction. The amount of mixing and product formation, the effects of the Reynolds number and chemical reaction rate, and the structure of the reacting layer prior to the mixing transition are some of the issues addressed in these investigations. Models of the mixing and chemical reaction under these conditions were proposed by Marble & Broadwell (1977) and by Broadwell & Breidenthal (1982) and Broadwell & Mungal (1991). On the numerical side, Riley, Metcalfe & Orszag (1986) carried out three-dimensional simulations of a temporally-evolving constant density flow with a single-step temperature-independent chemical reaction and showed that their results agree with similarity theory and compare well with the experimental data of Mungal & Dimotakis. Givi, Jou & Metcalfe (1986) addressed the problem of local extinction of a single-step irreversible Arrhenius reaction by means of two-dimensional temporally evolving simulations, and Ghoniem & Givi (1988) used the same kinetics in a two-dimensional spatially evolving simulation. A simulation of the spatially evolving flow with an infinitely fast reaction was performed by Delhaye *et al.* (1994), who also proposed a model based on an equation for the mean flame surface density and a description of the strained flame elements.

The effect of heat release on the flow was investigated by Wallace (1981), using the nitric oxide-ozone reaction with adiabatic temperatures up to 700 K and, more thoroughly, by Hermanson & Dimotakis (1989). They used the hydrogen-fluorine reaction with adiabatic temperatures ranging from 486 to 1240 K and showed that the growth rate of the layer, the turbulent shear stresses, and the overall entrainment are reduced as a consequence of the heat release. They also found that large-scale structures persisted in their experiment, but the mean structure space scaled with the layer width decreased with increasing heat release, which led these authors to suggest that the mechanisms of large-structure coalescence are inhibited by heat release. A review of further experimental work can be found in Dimotakis (1991).

McMurtry *et al.* (1986) studied the coupling between chemical heat release and fluid dynamics by means of direct numerical simulations of a two-dimensional, temporally evolving mixing layer with a single-step, irreversible exothermic reaction independent of the temperature. Using a zero Mach number formulation, they found that the rate of product generation, the thickness of the mixing layer, and the vorticity at the center of the vortex structures all decrease with increasing rates of heat release. They analyzed the influence of the baroclinic torque, pointing out that it changes sign across the flame because the direction of the pressure gradient in the high temperature region is roughly radially outward from the centers of the vortices, while the density gradient changes sign across the reaction front. As the flow evolves, this results in the generation of vorticity that alternately opposes and enhances the original vorticity, leading to several local extremas and to a vorticity distribution more diffuse than for a constant density fluid. McMurtry,

Riley & Metcalfe (1989) confirmed these results in a three-dimensional simulation and found that the Reynolds stresses, the turbulent kinetic energy, and the three-dimensionality of the flow also decrease with increasing heat release, in agreement with the experimental results of Hermanson & Dimotakis. Similar results were obtained by Grinstein & Kailasanath (1992) in a two-dimensional simulation of a compressible subsonic spatially evolving mixing layer.

Extensive simulations of compressible and/or reacting mixing layers have been carried out by Planché & Reynolds (1992) using an exothermic Arrhenius kinetics and values of the equivalence ratio such that the flame is near the center of the layer. They found that this flow behaves as two independent colayers separated by an approximately plane flame. Mixing occurs only between fuel and combustion products on one side of the layer and between oxidizer and products on the other side, but no roll-up or pairing was seen. Instead, the authors propose that the modification of the mean flow by the structures of each colayer causes the decay of these structures and the emergence of new ones of larger scale, which results in a slow growth of the layer.

The purpose of this work is to investigate in further detail the effect of chemical heat release on the first stages of the development of a plane mixing layer at zero Mach number. As in much previous work, we restrict ourselves to two-dimensional numerical simulations, which should provide valuable information since it is abundantly clear that these early stages are dominated by the dynamics of large-scale two-dimensional structures. The chemical reaction takes place between two unmixed species and the reaction time is supposed to be much shorter than the shortest time scale of the flow, so that the molecular mixing of the reactants is confined to a continuous infinitely thin diffusion flame. This assumption leaves out many important phenomena related to ignition and extinction but, in its broad range of applicability, gives results independent of any specific reaction law and renders the numerical resolution of the reaction zone unnecessary. A further limitation comes from the temporally evolving nature of the computations, which leaves out the effects of entrainment asymmetry (see, e.g., Dimotakis 1986 for a discussion of entrainment) and feedback from the downstream flow. While both effects are very important for a real reacting mixing layer, we expect that the temporally evolving flow still contains the essential ingredients of the internal dynamics of the mixing layer. As for the results, while a drastic reduction of the efficiency of the large-scale mixing seems to be unavoidable for non-small Mach numbers or when the flame sits near the center of the mixing layer, we find that this is not necessarily the case for the relatively high values of the effective stoichiometric ratio (or equivalence ratio) and initial vorticity distributions typical of many practical combustion systems. In this case, the mean location of the flame is displaced toward the oxidizer side and the presence of low density fluid modifies the evolution of the vorticity without suppressing the roll-up and pairing processes typical of constant density mixing layers.

2. Formulation and numerical method

Consider a plane two-dimensional temporally evolving unconfined mixing layer between a gas stream of velocity U and temperature T_o carrying a mass fraction $y_{o\infty}$

of an oxidizer and another gas stream of velocity $-U$ and temperature T_f carrying a mass fraction $y_{f\infty}$ of a fuel. The two species react in an exothermic infinitely fast chemical reaction so that a diffusion flame exists in the mixing layer where an amount of heat Q is released per unit mass of burned fuel. The velocity U is much smaller than the speeds of sound in either stream so that compressibility effects are negligible, but the density and temperature of the gas change due to the heat release (and to the temperature difference between the two streams if $T_f \neq T_o$).

In what follows the velocities and lengths are scaled with U and $\delta_\omega = 2U/\max(\partial\overline{u}/\partial y)_0$, the vorticity thickness of the initial mean flow, the temperatures and densities with the fuel-stream values T_f and ρ_f, and the pressure with $\rho_f U^2$.

The mass and momentum conservation equations are

$$\frac{\partial \rho}{\partial t} + \nabla \cdot (\rho \mathbf{v}) = 0 \ , \tag{1}$$

$$\frac{\partial}{\partial t}(\rho \mathbf{v}) + \nabla \cdot (\rho \mathbf{v}\mathbf{v}) = -\nabla p + \frac{1}{Re}\{\nabla \cdot (\tilde{\mu}\nabla \mathbf{v}) + \mathbf{N}\} \ , \tag{2}$$

where $Re = \rho_f U \delta_\omega / \mu_f$ is the Reynolds number, $\tilde{\mu} = \mu/\mu_f$ depends only on the temperature: $\tilde{\mu} = T^\sigma$,

$$\mathbf{N} = \begin{pmatrix} \tilde{\mu}_y v_x - \tilde{\mu}_x v_y \\ \tilde{\mu}_x u_y - \tilde{\mu}_y u_x \end{pmatrix} \ ,$$

and the normal viscous stress $Re^{-1}(\tilde{\mu}_v + \tilde{\mu}/3)\nabla \cdot \mathbf{v}$ is included in the pressure.

In the limit of zero Mach number, and neglecting the variations of the mean molecular mass of the gas mixture, the equation of state is

$$\rho T = 1 \ . \tag{3}$$

The velocity and pressure are L-periodic functions of the streamwise coordinate x (the choice of the period is discussed later) and satisfy

$$u \to \pm 1 \ , \qquad \rho v \to \alpha_\pm \phi \ , \qquad \frac{\partial p}{\partial y} \to \mp \alpha_\pm \frac{\partial \phi}{\partial t} \qquad \text{for} \qquad y \to \pm\infty \ , \tag{4}$$

where $\phi = \frac{1}{L}\int_0^L \int_{-\infty}^{\infty} \frac{\partial \rho}{\partial t}\, dx\, dy$ is the outflow due to the gas expansion, which is split between the two sides of the mixing layer by means of the factors $\alpha_+ = 1/(1+T_o^{1/2})$ and $\alpha_- = \alpha_+ - 1$. These values result from matching the mixing layer to outer wave regions where acoustic effects would be important.

Assuming that the Lewis numbers of the two species are equal to unity, the energy and species conservation equations are

$$L(T) = \frac{Q}{c_p T_f} w \ , \qquad L(y_f) = -w \ , \qquad L(y_o) = -sw \ , \tag{5a,b,c}$$

where

$$L(*) = \frac{\partial}{\partial t}(\rho *) + \nabla \cdot (\rho \mathbf{v} *) - \frac{1}{RePr}\nabla \cdot (\tilde{\mu}\nabla *) \ , \tag{6}$$

y_f and y_o are the mass fractions of fuel and oxidizer, $\rho_f U w/\delta_\omega$ is the mass of fuel consumed per unit volume per unit time, s is the mass of oxidizer required to burn the unit mass of fuel ($s = \mathrm{M}_o\nu/\mathrm{M}_f$ for the overall reaction $F + \nu O \rightarrow products$, where M_f and M_o are the molecular masses of the two species), and c_p and Pr are the specific heat at constant pressure and the Prandtl number, both assumed constant.

As can be seen by combining (5b)–(5c) and (5a)–(5b), the mixture fraction and the modified enthalpy, $(SY_f - Y_o + 1)/(1 + S)$ and $(T - T_o + qY_f)/(1 - T_o + q)$ respectively, satisfy transport equations similar to (5) but without reaction terms in the right hand sides (Williams 1985). Here $Y_f = y_f/y_{f\infty}$ and $Y_o = y_o/y_{o\infty}$, $S = sy_{f\infty}/y_{o\infty}$ is the effective stoichiometric ratio, and $q = Qy_{f\infty}/c_pT_f$. In addition, both variables satisfy the same boundary conditions and, assuming that the initial conditions are also the same, we find that

$$\frac{SY_f - Y_o + 1}{1 + S} = \frac{T - T_o + qY_f}{1 - T_o + q} \equiv Z(x, y, t) \tag{7}$$

satisfies

$$L(Z) = 0 \ , \tag{8}$$

and

$$\begin{aligned} Z &= 0 \quad \text{for} \quad y \rightarrow \infty \\ Z &= 1 \quad \text{for} \quad y \rightarrow -\infty \\ Z(x, y, t) &= Z(x + L, y, t). \end{aligned} \tag{9}$$

In the Burke-Schumann limit of diffusion-controlled flames eqs. (5a-c) yield $w = 0$ to leading order (see Williams 1985 for details). The precise form of the consumption rate need not by specified in this limit other than requiring that $w = 0$ implies

$$Y_f Y_o = 0 \ , \tag{10}$$

which means that the two reactants do not coexist, being separated by an infinitely thin flame where both concentrations vanish. Eqs. (7) and (10) suffice then to determine the temperature and species concentrations in terms of the mixture fraction Z. At the flame the mixture fraction and temperature take the values

$$Z_{st} = \frac{1}{1 + S} \qquad \text{and} \qquad T_{ad} = T_o + \frac{1 - T_o + q}{1 + S} \ , \tag{11}$$

and

$$\begin{array}{llll} Y_f = \frac{Z/Z_{st} - 1}{S} \ , & Y_o = 0 \ , & T = 1 + (T_{ad} - 1)\frac{1 - Z}{SZ_{st}} & \text{for} \quad Z > Z_{st} \\ Y_f = 0 \ , & Y_o = 1 - \frac{Z}{Z_{st}} \ , & T = T_o + (1 - T_o + q)Z & \text{for} \quad Z < Z_{st} \end{array} \tag{12}$$

Notice that since Z and its first derivatives are continuous across the flame, the gradients of oxidizer and fuel concentrations and the gradients of temperature on either side of the flame verify

$$\left.\frac{\partial Y_o}{\partial n}\right|_+ = -S \left.\frac{\partial Y_f}{\partial n}\right|_- \qquad \text{and} \qquad \left.\frac{\partial T}{\partial n}\right|_+ = \left.\frac{\partial T}{\partial n}\right|_- + q \left.\frac{\partial Y_f}{\partial n}\right|_- , \qquad (13a,b)$$

where n is the normal to the flame.

The problem (1)–(4), (8), (9), and (12) is to be solved subject to the initial conditions discussed in the following section.

For the numerical treatment, a second order finite volume method on a staggered grid is used for eqs. (1), (2), and (8). The time integration, which is also second order accurate, is explicit for the convection terms, implicit for the transport terms, and uses a time splitting for the pressure correction. This amounts to the standard decomposition $(\rho\mathbf{v})^{(n+1)} - (\rho\mathbf{v})^{(n)} = \delta_1(\rho\mathbf{v}) - \Delta t \nabla \delta p$, and (1) yields

$$\Delta t \nabla^2 \delta p = \left(\frac{\partial \rho}{\partial t}\right)^{(n+1)} + \nabla \cdot \left[(\rho\mathbf{v})^{(n)} + \delta_1(\rho\mathbf{v})\right] . \qquad (14)$$

The only difference with respect to a constant density fluid is the presence of $(\partial\rho/\partial t)^{(n+1)}$ in the right hand side of (14). Since $\rho = \rho(Z)$, by (3) and (12), this term can be computed by evaluating (8) at the time level $(n+1)$. However $(\rho\mathbf{v}Z)^{(n+1)}$ in the convection term of this equation gives the unknown contribution

$$\Delta t \frac{\nabla \cdot (Z^{(n+1)} \delta p)}{\left(\frac{\rho}{d\rho/dZ} + Z\right)^{(n+1)}}$$

along with others already known ($Z^{(n+1)}$ is already known from the solution of (8), which can be computed before solving (14)). Thus, when this $(\partial\rho/\partial t)^{(n+1)}$ is carried into (14) and into the boundary condition (4) for v, an elliptic problem results for δp which differs from the usual one for a liquid. This problem is solved iteratively at each time step.

Eq. (12) implies $dT/dZ = (1 - T_o + q) - (q/SZ_{st})H(Z - Z_{st})$, where $H(\zeta)$ is the Heaviside step function. In the numerical simulations, the discontinuity of the temperature derivative at the flame was smoothed out replacing $H(\zeta)$ by $H_\beta(\zeta) = [\tanh(\beta\zeta) + 1]/2$ and then, to the same approximation, $T(Z) = T_{ad} - (q/\beta S Z_{st}) \ln 2^{1/2} + \int_{Z_{st}}^{Z} (dT/dZ')\, dZ'$, which becomes exact when $\beta \to \infty$. This approximation amounts to assigning a finite thickness to the flame, measured by β^{-1}. It was checked that the results do not depend on β provided it is sufficiently large for the transport effects to dominate in the scale of this artificial thickness. Typically $\beta = 20$ in the computations presented below.

3. Initial conditions and linear stability

The initial conditions are the superposition of a base flow independent of x and small perturbations proportional to the eigenfunctions of the most unstable mode and its subharmonic, as given by a linear stability analysis of the base flow.

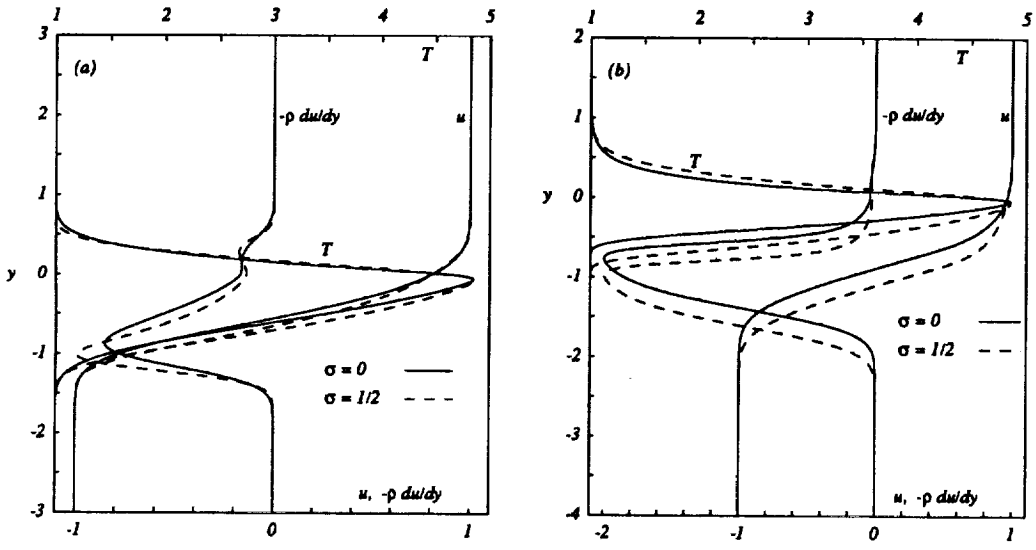

FIGURE 1. Temperature, velocity, and density-weighted vorticity for: (*a*) first type of base flow, and (*b*) second type of base flow.

Two kinds of base flows are considered. The first is the result of letting an initial state consisting of a halfspace with $Z = 0$ and another with $Z = 1$, each moving with opposite velocities parallel to their common boundary evolve for a finite time t. This leads to a self-similar flow in which the mixture fraction and the streamwise velocity are of the form $Z = Z(\eta)$ and $u = U(\eta)$ with $\eta = \xi/t^{1/2}$ and $\xi = \int^y \rho\, dy$, and satisfy

$$[F(Z)Z_\eta] + \frac{Pr}{2}\eta Z_\eta = 0 \ , \tag{15a}$$

$$[F(Z)U_\eta] + \frac{1}{2}\eta U_\eta = 0 \ , \tag{15b}$$

$$Z = 0 \ , \quad U = 1 \qquad \text{for} \quad \eta \to \infty \ , \tag{15c}$$

$$Z = 1 \ , \quad U = -1 \qquad \text{for} \quad \eta \to -\infty \ , \tag{15d}$$

where $F(Z) = T^{\sigma-1}$ with $T(Z)$ given by (12), rounded as commented at the end of the previous section. The extra condition $Z(0) = Z_{st}$ is used to fix the origin; it amounts to measuring transverse distances from the flame. The transverse velocity, $O(1/\sqrt{Re\, t})$, due to the gas expansion, and the pressure are computed afterward from the equations of motion and the boundary conditions (4). The nondimensional vorticity thickness of this flow is $\delta_\omega = 2(t/Re)^{1/2}/\max_\eta(\rho U_\eta)$, and the condition $\delta_\omega = 1$ determines the value of t in the previous expressions. The resulting profiles for $q = 40$, $S = 9$, and $Pr = 1$ are plotted in Fig. 1a. Notice that the flame (at $y = 0$) is displaced toward the oxidizer side of the mixing layer. This is because the oxidizer and fuel diffusion fluxes must satisfy (13a) and, for the present moderately large S, this is possible only if the flame is in a region of small fuel concentration.

The previous solutions give vorticity and mixture fraction profiles of similar thickness when $Pr = O(1)$. This, however, is not a realistic representation of situations in which one or the two streams have been flowing parallel to a splitter plate or channel wall before forming the mixing layer. Then the vorticity at a short distance downstream the edge of the plate spreads over a boundary layer whose thickness depends on the length of the solid wall, whereas the diffusion of the species and the heat begins only around the trailing edge of the plate and extends therefore to a thinner sublayer. Assuming that the flow is laminar upstream, the thickness of this sublayer is $O(\epsilon^{1/3})$ in the nondimensional variables of the previous section, where $\epsilon = x/Re$ and x is the distance to the edge of the plate (Goldstein 1930). The structure of the laminar mixing layer for $Re \gg x \gg Re^{-1/2}$ (if only one of the fluids move) or for $Re \gg x \gg Re^{-1/4}$ (if the two fluids move) consists of a self-similar flow in this sublayer and one or two thicker layers of cold vortical flow. This solution can be computed by using asymptotic matching. Here, with a view to mimic the flow in the case of a stream of fuel discharging into stagnant oxidizer without having to construct a uniformly valid solution out of the different asymptotic expansions, we consider a base flow with velocity $u = 1 - 2df/d\xi$, where $f(\xi)$ and $Z(\xi)$ satisfy

$$\epsilon[F(Z)Z_\xi]_\xi + \frac{2}{3}PrfZ_\xi = 0 \ , \tag{16a}$$

$$\epsilon[F(Z)f_{\xi\xi}]_\xi + \left[\frac{2}{3}G + \frac{1}{2}\epsilon(1-G)\right]ff_\xi - \frac{1}{3}Gf_\xi{}^2 = 0 \ , \tag{16b}$$

$$Z = f_\xi = 0 \quad \text{for} \quad \xi \to \infty \ , \tag{16c}$$

$$Z = f_\xi = 1 \quad \text{for} \quad \xi \to -\infty \ , \tag{16d}$$

with

$$G = \frac{1}{2}\left\{1 + \tanh\left[\gamma\left(\xi_c^{3/2} + \frac{f}{f_\xi^{1/2}}\right)\right]\right\} \ ,$$

$1 \gg \xi_c \gg \epsilon^{1/3}$ and γ constants, and the condition $Z(0) = Z_{st}$ to fix the origin. Eqs. (16a,b) reduce to the ones describing Goldstein's self-similar flow in the distinguished limit $[f = \epsilon^{2/3}f_i, \xi = \epsilon^{1/3}\xi_i, (f_i, \xi_i) = O(1)]$ for $\epsilon \to 0$, in which $G \to 1$, and to Blasius' equation for an isothermal flow ($Z = 0$) in the distinguished limit $(f, \xi) = O(1)$ for $\epsilon \to 0$, in which $G \to 0$. Thus, in an approximate sense, the solution of (16) for small values of ϵ describes the whole flow. The artificial parameters $-\xi_c$ and γ control the position and abruptness of the transition between the two regions. Fig. 1b shows the solution of (16) for $q = 40$, $S = 9$, $Pr = 1$, $\epsilon = 2.2\text{x}10^{-3}$, $\xi_c = 0.33$, and $\gamma = 1$, normalized to have $\delta_\omega = 1$.

A linear stability analysis of both types of flows is carried out using the parallel flow approximation and neglecting transport effects for the perturbations. Squire's theorem holds for these zero Mach number flows and, therefore, it suffices to consider planar perturbations of the form $u = u_s(y) + \Delta u(x, y)$, etc., where the subscript s denotes here the base flow and $\Delta u(x, y) = \hat{u}(y)\exp[i\alpha(x - ct)] \ll 1$, with α real

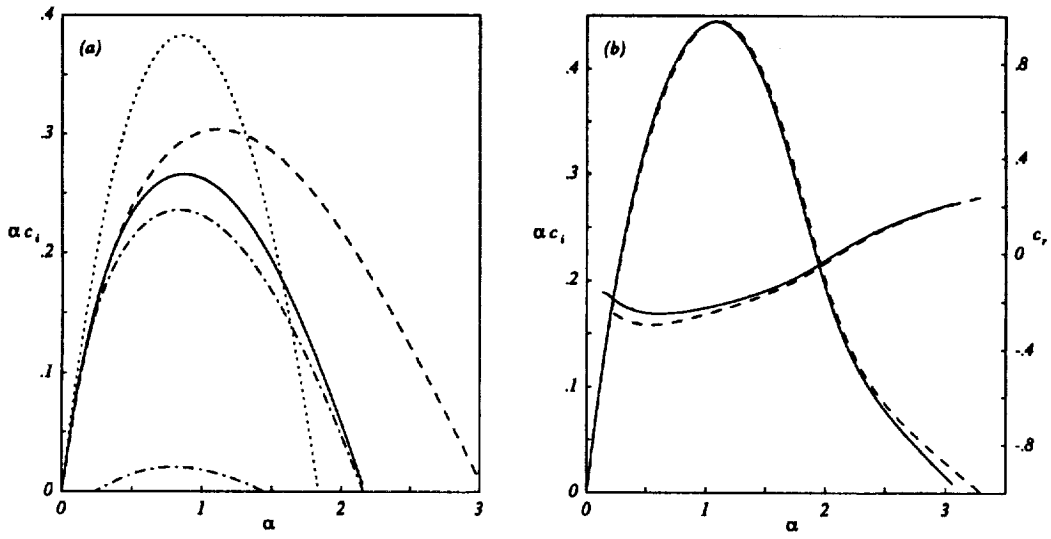

FIGURE 2. Growth rate as a function of the wave number for (a) the first type of base flow and (b) the second type of base flow. In (a), the cases depicted are ——— , $q = 40$, $S = 9$, $\sigma = 0$; ---- , $q = 40$, $S = 9$, $\sigma = 1/2$; —·— , $q = 20$, $S = 4$, $\sigma = 0$; and ····· , $q = 0$. In (b) the cases depicted are ——— , $q = 40$, $S = 9$, $\sigma = 0$; and ---- : $q = 40$, $S = 9$, $\sigma = 1/2$, and the phase speed is on the right-hand scale.

and c complex. After standard manipulations of the linearized equations, we end up with the eigenvalue problem

$$\begin{aligned} &(u_s - c)\left[(\rho_s \hat{v}')' - \rho_s \alpha^2 \hat{v}\right] - (\rho_s u_s')' \hat{v} = 0 \ , \\ &\hat{v} \to 0 \qquad \text{for} \quad y \to \pm\infty \ , \end{aligned} \tag{17}$$

where $\hat{v}$ is the transverse velocity perturbation. The resulting growth rate (αc_i) as a function of the wave number is plotted in Fig. 2a for several base flows of the first type discussed above and in Fig. 2b for base flows of the second type.

It was pointed out by Shin & Ferziger (1991) and Planché & Reynolds (1992) that the density-weighted vorticity $-\rho_s u_s'$ plays to a large extent the same role as the vorticity for a constant density flow. This quantity has two distinct peaks for sufficiently exothermic reactions with values of S not far from one, leading to two different unstable modes for a range of α bounded away from zero. Each mode is associated with one of the peaks and has a phase velocity closer to the velocity of the stream nearer to that peak. A remnant of the two peaks can be seen in Fig. 1a, and two unstable modes still exist for $q = 20$, $S = 4$ (Fig. 2a). However, the lower peak dominates for higher values of S, leaving only one unstable mode for each wave number. The corresponding eigenfunctions have their extremes around the flame position and around the peak of the weighted vorticity.

Another important feature is that the phase velocity of the perturbations depends on the wave number; it is negative for the cases of Fig. 2a and, contrarily to what

Case	σ ($\mu \propto T^\sigma$)	A_1	A_2	φ_1	Re	Base Flow
(a)	0.0	0.05	0.05	0	1000	1
(b)	0.0	0.15	0.05	0	1000	1
(c)	0.5	0.05	0.05	0	1000	1
(d)	0.5	0.15	0.05	0	1000	1
(e)	0.5	0.15	0.05	$\pi/2$	1000	1
(f)	0.5	0.15	0.05	0	2000	1
(C)	0.5	0.05	0.05	0	1000	2
(D)	0.5	0.15	0.05	0	1000	2

Table 1. Conditions for the various cases run. A_1 and A_2 are the subharmonic and fundamental amplitudes (see text) and φ_1 is the relative phase of the subharmonic. Base flow types (1 and 2) are described in §3.

can be seen in Fig. 2b, its absolute value increases with α. In general, the maximum growth rate increases by decreasing q or increasing S.

4. Numerical results and discussion

In all the cases discussed in this section the temperature of the two streams are equal ($T_o = 1$) and, unless otherwise specified, $q = 40$ and $S = 9$, leading to an adiabatic temperature of 5 times the free-stream temperature. This relatively high value of S is typical of many real situations; e.g., $S \sim 15$ for hydrocarbons burning in air. The Reynolds number is 1000 in all the computations except case (f) below, and $Pr = 1$. The length L of the computational domain is twice the wavelength of the most amplified small perturbation for the corresponding base flow. The initial perturbation is given by the eigenfunction of this mode normalized so that $\max|\hat{u}| = 1$ and multiplied by the amplitude $A_2 = 0.05$ plus that of its subharmonic taken with various amplitudes (A_1) and phases (φ_1). The specific conditions of each case are listed in the Table. The cross-stream boundary conditions are applied at $y = \pm 8$ in computations with the first type of initial conditions and at $y = -9$ and $y = 7$ in computations with the second type of initial conditions.

4.1. Global results

Global results for a number of simulations carried out with the first type of initial conditions are displayed in Fig. 3. Fig. 3a shows the time evolution of the mean momentum thickness ($\delta_m = \int_{-\infty}^{\infty}(1 - \overline{\rho}\,\overline{u}^2)\,dy$, the overbar meaning streamwise average) scaled with its initial value. As can be seen, the growth rate of the mixing layer is similar for all the cases displayed, and smaller than for a constant density fluid. Fig. 3b shows the overall rate of product generation (W),

$$W = \frac{1}{L}\int w\,dx\,dy = \frac{1}{L}\frac{d}{dt}\int \rho\tilde{Y}_p\,dx\,dy,$$

where

$$\tilde{Y}_p = \begin{cases} (1-Z)/(1-Z_{st}) & \text{if } Z > Z_{st}; \\ Z/Z_{st} & \text{if } Z < Z_{st}; \end{cases}$$

is proportional to the product mass fraction. Figs. 3c and 3d show the first two Fourier modes of the transversely averaged kinetic energy

$$E_k = \frac{1}{2}\int_{-\infty}^{\infty} \left\{ \left(\widehat{\rho^{1/2}u}\right)^2(k,y) + \left(\widehat{\rho^{1/2}v}\right)^2(k,y) \right\} dy \ ,$$

where the hat denotes streamwise Fourier transform. The modes in Figs. 3c-d correspond to the wave numbers of the most amplified perturbation ($k = 2$) and its subharmonic ($k = 1$).

The first peaks of the curves of Fig. 3c represent the roll-up of the vortices, which is accompanied by a first maximum of the product generation, and the first peaks of the curves of Fig. 3d represent the amalgamation of pairs of vortices. Cases (a) and (b) correspond to a constant viscosity fluid ($\sigma = 0$) with the amplitude of the subharmonic $A_1 = 0.05$ and 0.15, respectively. The amalgamation occurs earlier and the reaction rate has a tall peak shortly after the maximum of E_1 when the amplitude of the subharmonic is larger. Cases (c) and (d) are the analogs of (a) and (b) with a variable viscosity fluid ($\sigma = 0.5$), whereas case (e) differs from (d) only by a $\pi/2$ shift in the phase of the subharmonic. The effect of the initial phase shift is less obvious here than for a constant density fluid because the phase speed of the perturbations depends on the wave number and, therefore, the phase shift changes with time. However, a strong influence remains, as the change in phase results in a delay in the amalgamation and suppresses the tall peak of the rate of product generation. Case (f) has the same initial conditions as (d) but $Re = 2000$. The differences between the two reflect the influence of the viscosity, which may be strong at $Re = 1000$, especially when the viscosity increases with temperature.

In none of the cases presented does the flame sheet enter the cores of the vortices, and its surface never increases very much. This is because the relation (13a) implies that the flame must always be in regions of small fuel concentration since S is moderately large, and such regions are not easily ingested by the vortices when cushioned by a layer of low density fluid (see next subsection). Similarly, owing to (13b), the temperature gradient on the oxidizer side must be much larger than on the fuel side when q is large, a fact that is confirmed in Figs. 5 and 6 below. Under these conditions, the peaks along the flame in the product generation rate are due to the enhancement of the diffusion fluxes in regions of high strain on the flame surface. The strong dependence of this strain (and therefore the rate of product generation) on the amplitude and phase of the initial perturbations suggests that it is possible to control the combustion by manipulating the flow.

Further computations were carried out decreasing q (hence the flame temperature) at constant S, and decreasing q and S simultaneously to bring the flame closer to the center of the mixing layer while keeping the flame temperature constant. The results of the first series of computations, similar to (a) but with q equal to 20 and 30, show features approaching those of an incompressible flow as q decreases: the

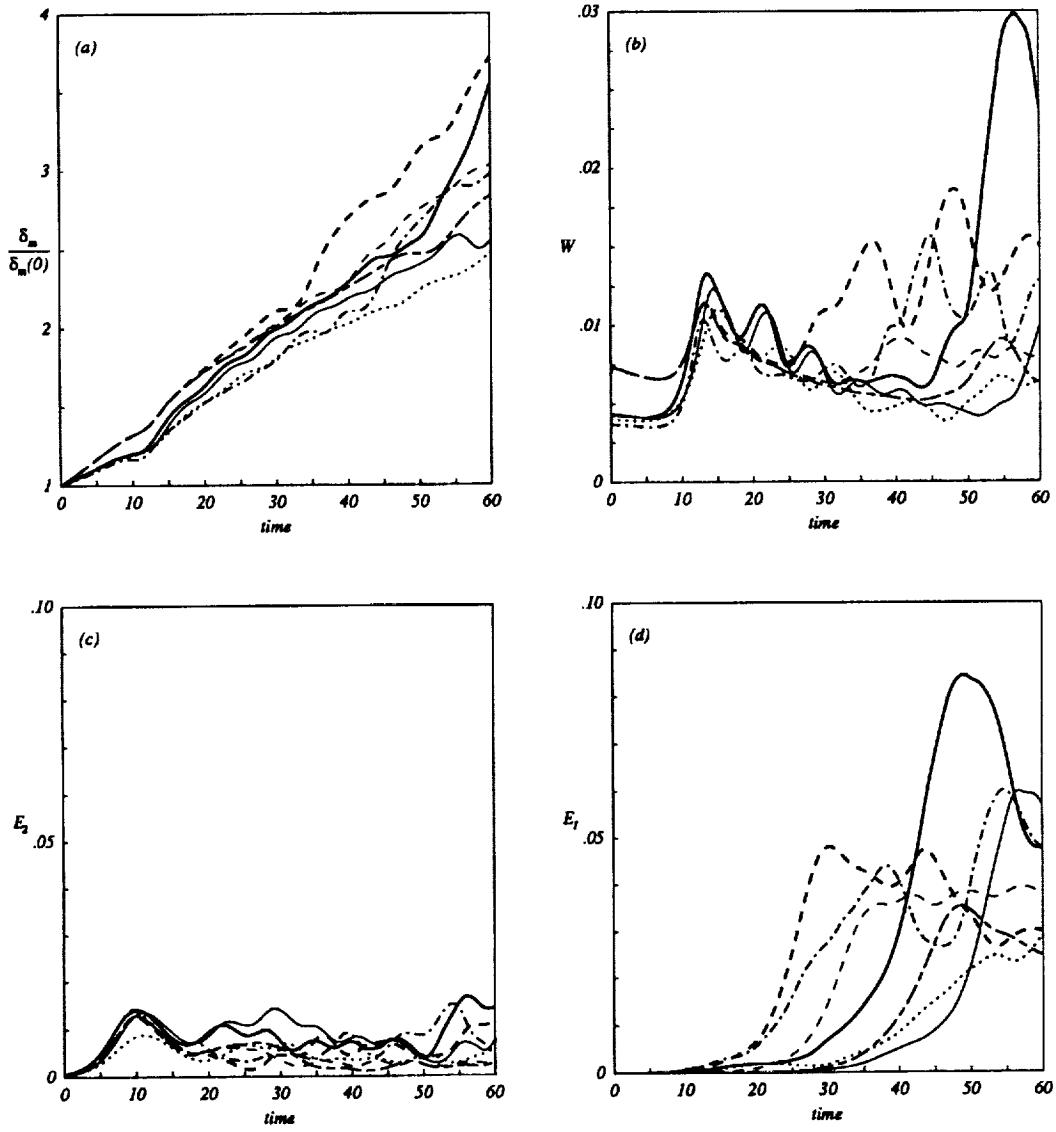

FIGURE 3. Evolution of (a) the scaled momentum thickness, (b) the overall rate of product generation, (c) the kinetic energy in the second Fourier mode, and (d) the kinetic energy in the first Fourier mode, for cases: —— (a); —— (b); - - - - (c); - - - - (d); — - — (e); — · — (f); ····· (g).

vortices get rounder than in Fig. 5 below, the layer grows faster, and the fuel lean region containing the flame is more easily wrinkled and stretched by the flow, which results in higher rates of product generation. The second series of computations, $(q, S) = (20, 4)$, $(12, 2)$, and $(8, 1)$, show that the amalgamation is retarded or suppressed and the rate of product generation decays with oscillations after peaking at

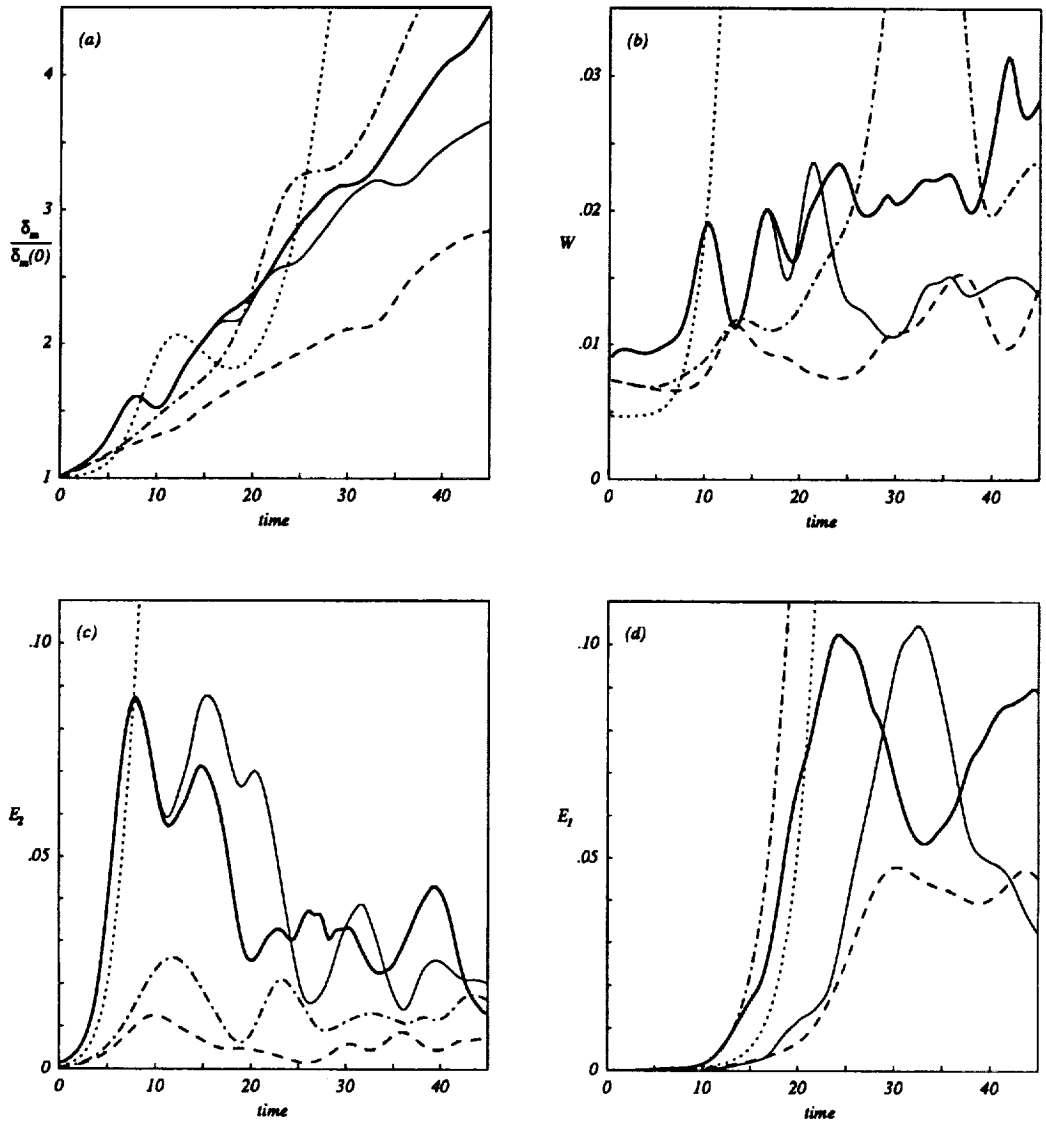

FIGURE 4. Evolution of (a) the scaled momentum thickness, (b) the overall rate of product generation, (c) the kinetic energy in the second Fourier mode, and (d) the kinetic energy in the first Fourier mode, for cases: —— (C); —— (D); ---- (d); —·— (d'); and ····· a constant density flow.

roll-up when S begins to decrease (case (g) in Fig. 3b is the first case of this series; for still smaller values of S the roll-up also disappears, apparently giving way to the two-colayers regime discussed by Planché & Reynolds (1992)).

Fig. 4 shows the same quantities as Fig. 3 for two runs carried out with initial conditions of the second type: cases (C) and (D) are analogous to (c) and (d); i.e.,

$\sigma = 1/2$ and the amplitude of the subharmonic equal to 0.05 and 0.15, respectively. For comparison, the results of case (d) have been repeated in this figure (dashed lines), and the results for a constant density fluid ($q = 0$, $S = 9$) have also been included (dotted lines). Finally the dash-and-dot lines correspond to case (d') discussed below. As can be seen, the growth of the mixing layer is faster than for the first type of initial conditions, and similar to that of a constant density fluid for times up to about 20. The amplitude of the second mode of the kinetic energy (E_2) is also higher, of the order of the amplitude of the first mode (E_1), reflecting a more efficient roll-up and the presence of round vortices at least during part of the evolution. The two peaks of E_2 reflect another characteristic feature of this flow that will be commented on below.

4.2. Mechanics of the flow

Fig. 5 shows the evolution of the vorticity and the temperature for case (f), which is typical of the first type of initial conditions. In accordance with the results of the linear analysis, the vortices move with a velocity closer to that of the fuel stream (the lower stream in Fig. 5) than to that of the oxidizer stream (the structures move to the left). Furthermore, the interaction of the vortical region of the layer with the fuel side (lower) is typical of the constant density flow, with large excursions of free-stream fluid into the layer, whereas on the oxidizer side (where the flame is), these large-scale incursions are not so pronounced. The hydrodynamic mixing layer grows by entraining free-stream fluid as the vortices roll-up and amalgamate. On the oxidizer side, however, the heat release of the flame and the associated volumetric expansion of the surrounding fluid acts as a source of fluid volume to be entrained. Thus this low-density fluid below the flame, which is easier to entrain than the free-stream cold fluid, acts as a buffer between the mixing layer and the flame, inhibiting the entrainment of the flame and free-stream fluid.

The light fluid enters each vortex in the form of a jet to its upper right, turns around the vortex to the left on the lower side, and splits into a recirculating flow around the vortex core and a blob of light fluid that leaves the vortex to the lower left ($t = 9$ to 15). The heavy fluid entering a vortex at its lower left turns over the top to the right and tends to escape as a tongue by its upper right ($t = 15$). The light fluid appears to be more easily turned and engulfed by the vortices than the heavy fluid, as might be expected given the difference in density. The right-ward moving tongue at the top throttles the ingestion of new light fluid from the upper right ($t = 15$), and similarly, the left-ward moving blob of light fluid temporarily suspends the ingestion of new heavy fluid.

The general effect of these combined motions of light and heavy fluid is to make the temperature field structures more elongated than for a constant density fluid. The numerical results show a variety of situations depending on the order in which the supplies of light and heavy fluid to a given vortex are interrupted and restored, which in turn depends on the initial conditions and on the Reynolds number. The supply of light fluid can be interrupted more than once before two neighboring vortices amalgamate. Thus, in case (b) (not displayed), a tongue of heavy fluid separates completely from a vortex, restoring the ingestion of light fluid, but it

remains cold on leaping over the next vortex to the right (which is undergoing a similar evolution), so that, along with some newly ingested fluid from the lower stream, it throttles the supply of light fluid to this vortex for a second time. For their part, the blobs of light fluid in the lower part of the layer cool down while moving toward the left and undergo a further splitting in this case, being partially ingested by the next vortex to the left of that which shed the blob.

The right-ward motion of the tongues of heavy fluid over the vortices also determines the end of the roll-up process, and when this happens sections of the original vorticity layer are left unrolled between the tongues and the flame. It seems likely that through this mechanism the phase of the subharmonic in the initial condition may induce differences in the amount of vorticity rolled in each vortex and, thereby, in the subsequent evolution of the mixing layer. The unrolled vorticity patches correspond to regions of strong shear that move toward the right relative to the vortices, leap from vortex to vortex, and are selectively reinforced by the baroclinic torque. At sufficiently high Reynolds numbers some of these patches eventually roll up into secondary vortices located one or more periods to the right of the vortex to which they were initially tied (upper left of Fig. 5b at $t = 18$ to 21).

The evolution leading to the premature termination of the roll-up and the disruption of the rolled and unrolled vorticity can also be described in terms of the vorticity; see comments on Fig. 6 below. Here we note that in general the distributions of both $\nabla \times \mathbf{v}$ and $\nabla \cdot \mathbf{v}$ are required to reconstruct the velocity field. The vorticity is initially present in the flow, and its dynamics are essentially inviscid through convection and the baroclinic torque. In contrast, in the absence of compressibility effects, the changes in the density of a fluid particle are due to temperature changes, which are brought about by heat conduction. Thus at sufficiently high Reynolds numbers, heat conduction, and hence $\nabla \cdot \mathbf{v} = -\frac{1}{\rho}\frac{D\rho}{Dt}$, should be confined to very thin layers (which can only have a small effect on the large-scale dynamics of the flow) and, in a fully developed flow, to the smallest scales (which cannot influence the large-scale dynamics by this means because the net change of volume is negligible). This points toward a decreasing importance of $\nabla \cdot \mathbf{v}$ as the Reynolds number increases. Though $Re = 2000$ is probably not sufficiently high to claim independence of $\nabla \cdot \mathbf{v}$, the evolution depicted in Fig. 5 is probably more affected by the motion of the counterrotating vortex pairs that appear in the flow than by the dilatation or contraction of the fluid particles. Such pairs arise due to the baroclinic torque ($-\nabla T \times \nabla p$ in the vorticity equation), which, owing to the low pressure at the vortex centers, is positive in the lower halves of the light fluid jets entering the vortices and in most of the heated region above the flame, and negative in the upper halves of the jets and below the flame. This leads to production of positive vorticity in the former regions, which forms left-ward moving pairs with the rolled vorticity of the layer and, to a lesser extent, right-ward moving pairs with the unrolled vorticity.

It seems that in some cases, though not in the one displayed in Fig. 5, the unrolled layers of vorticity act as precursors to the amalgamation by establishing bridges

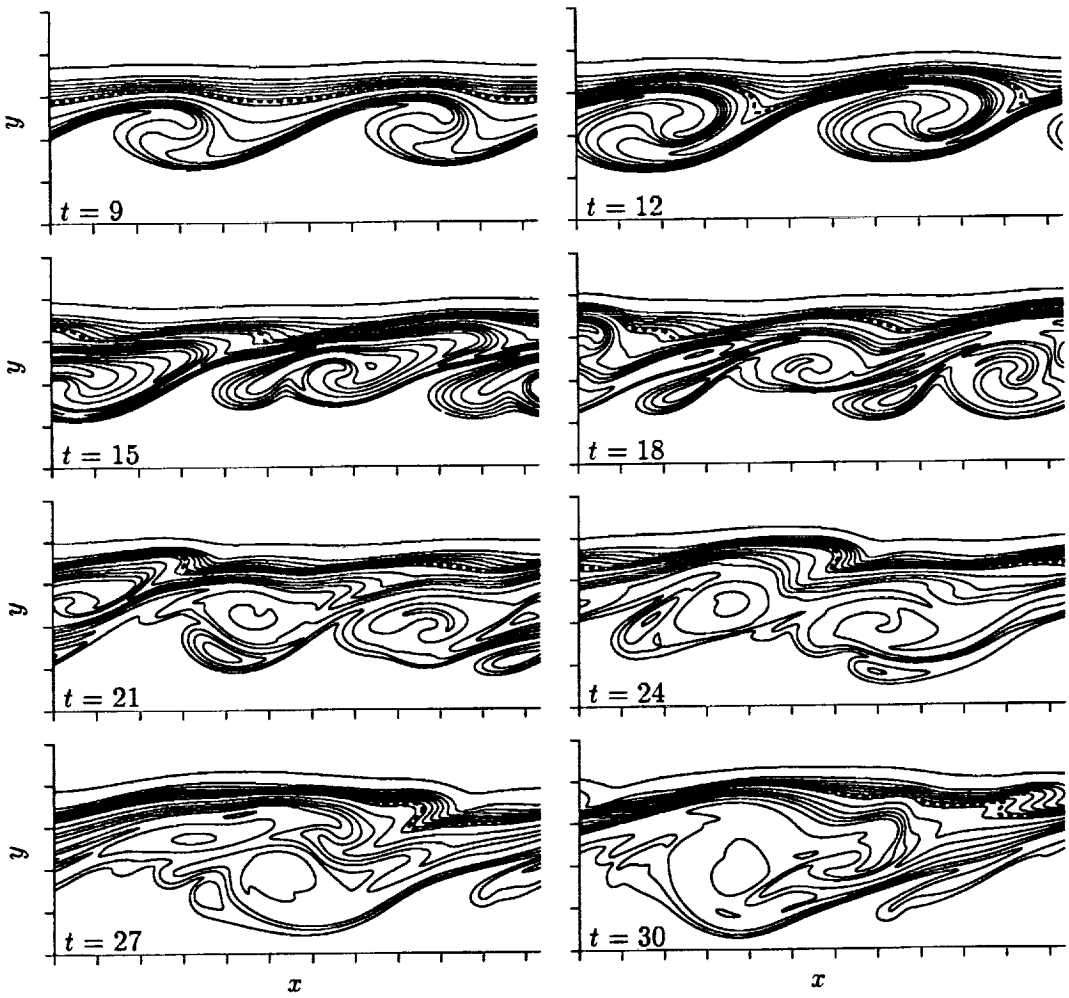

FIGURE 5(*a*). Evolution of the temperature in case (*f*). The contour increment is 0.5 and the free-stream temperature is 1. The flame location is indicated by the heavy dashed line.

between adjacent vortices with the right end of a bridge rolling around the vortex that will come to the bottom of the pair while the left end is still connected to the vortex that will come to the top. Any nearby secondary vortex that might have formed as well as the remnants of warm fluid blobs shed by other vortices are typically ingested in the amalgamation process.

The result of the amalgamation is a vortex much less organized than for a constant density fluid. It contains several vorticity peaks and layers of positive vorticity left over by the secondary vortices and vortex pairs that existed at earlier times ($t = 27$ to 30). However, the large-scale behavior of the new vortex does not differ qualitatively from that of the previous ones: as far as it can be followed in the

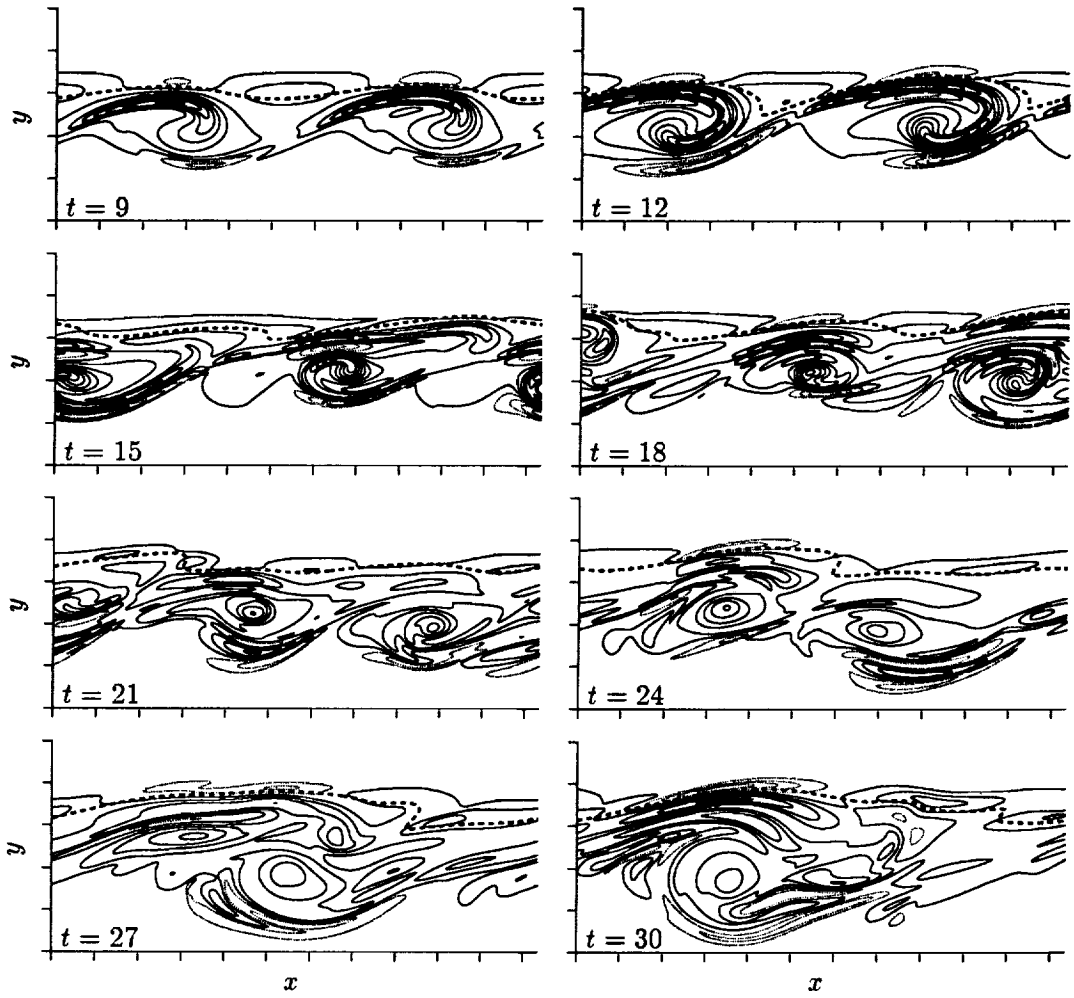

FIGURE 5(*b*). Evolution of the vorticity in case (*f*). The contour increment is 0.6 and positive contours are dotted. The flame location is indicated by the heavy dashed line.

present simulations, the vortex grows by ingesting light and heavy fluid until it ends up filling the computational domain.

To try to ascertain the importance of the baroclinic torque, the momentum Eq. (2) was artificially modified, replacing the pressure gradient term by $-\rho\nabla p$. This amounts to having a constant density fluid insofar as the pressure forces are concerned. No baroclinic term appears then in the vorticity equation (obtained by taking the curl of the modified momentum equation), but the term $-\omega\nabla\cdot\mathbf{v}$ due to the gas expansion is left unaltered, as well as the effect of $\nabla\cdot\mathbf{v}$ in the other conservation equations. Case (*d*) was rerun with this modification (it is denoted by (*d'*) in what follows) and some results are shown in Fig. 4 (dash-and-dot lines; the

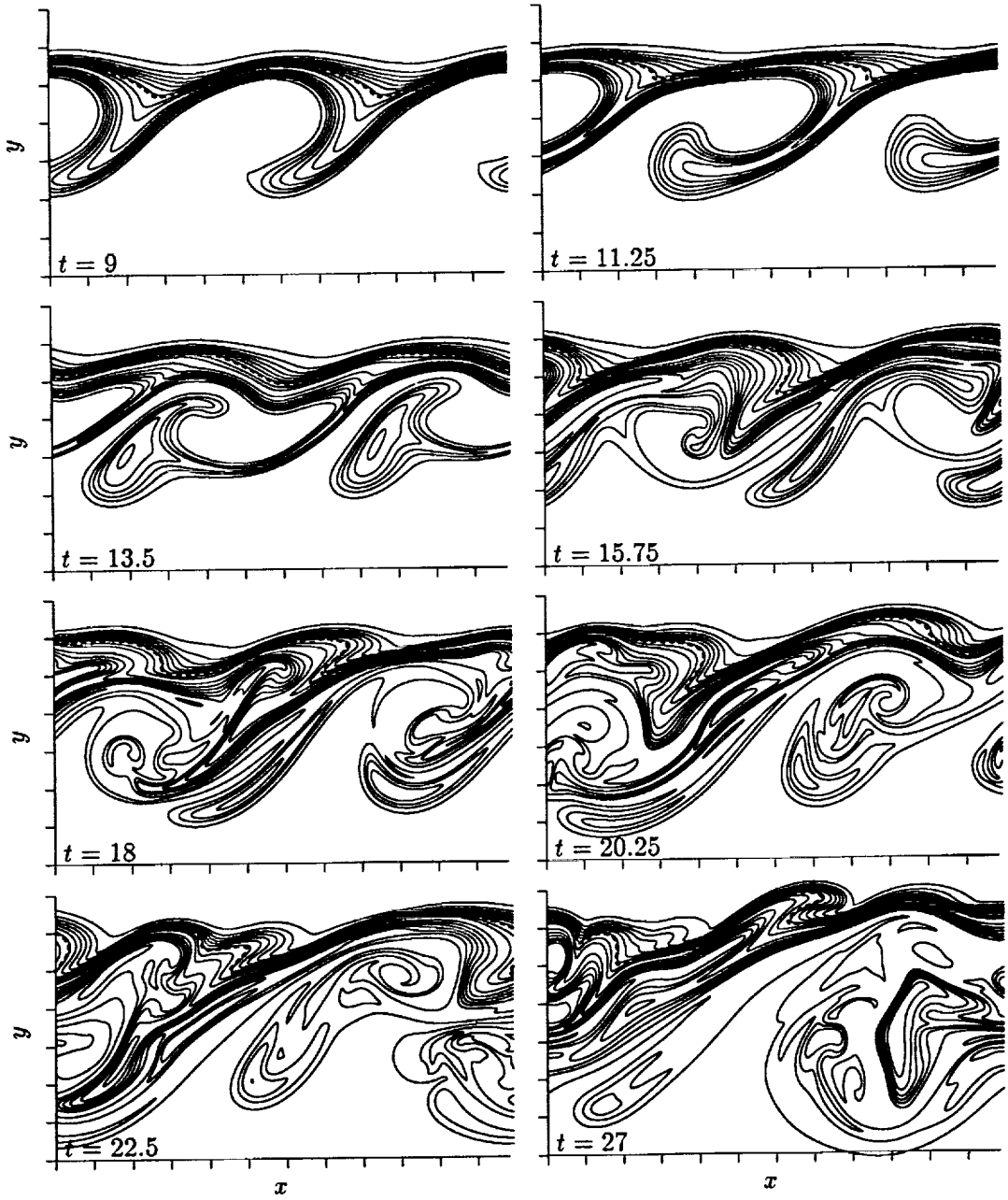

FIGURE 6(*a*). Evolution of the temperature in case (*D*). The contour increment is 0.5 and the free-stream temperature is 1. The flame location is indicated by the heavy dashed line.

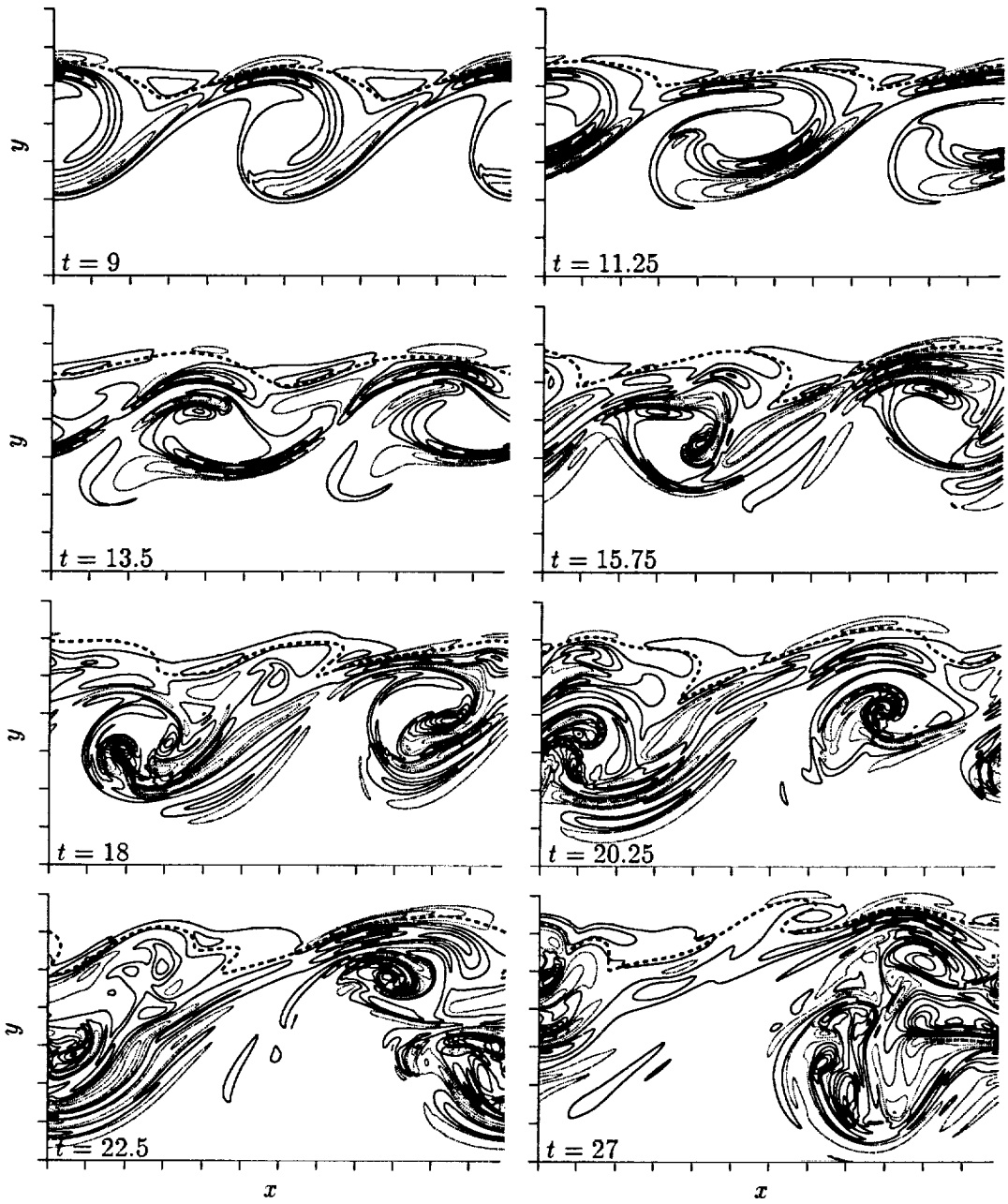

FIGURE 6(*b*). Evolution of the vorticity in case (*D*). The contour increment is 0.8 and positive contours are dotted. The flame location is indicated by the heavy dashed line.

dashed lines correspond to case (d)). As can be seen, the growth rate of the layer and the rate of product formation increase very much due to the modification, and inspection of the vorticity fields reveals that the vortices and the general appearance of the flow are closer to a constant density fluid than to case (d).

Fig. 6 shows the evolution of the vorticity and the temperature for case (D), the analog of (d) with an initial condition of the second type. Contrary to Fig. 5, the bulk of the initial vorticity is now in the low temperature fuel. The Kelvin-Helmholtz instability begins to develop as for a constant density fluid, leading to relatively round structures (for $t = 9$ and before) that are responsible for the first peak of E_2 in Fig. 4c. Very soon, however, the deflection of the light fluid around the flame leads to tongues where new vorticity is generated by the baroclinic torques in the form of counterrotating pairs. It is worth noting that this occurs in regions that would be relatively free of vorticity in a constant density fluid. The vortex pairs are more prominent than in Fig. 5 and clearly dominate the flow. They travel toward the left deep in the fuel stream ($t = 11.25$) before the dominant negative vorticity brings them back toward the shear layer, and in so doing, they make the elongated structures responsible for the dip of E_2 and engulf large amounts of cold fuel that are subsequently incorporated into the mixing layer. On returning to the shear layer, each of the regions of light fluid has the appearance of a mushroom with a very thin stalk. The high pressure above the cap of the mushroom splits it into a recirculating tongue and a shed blob, each with its associated vortex pair. The high pressure also squeezes substantial parts of the high temperature strip around the flame, increasing the diffusion fluxes and the burning rate while the parts of the strip between two pressure maxima get compressed and sucked by the depressions at the centers of the forming vortices. This leads to secondary tongues of light fluid (that begin forming at about $t = 13.5$ in Fig. 6a) where the baroclinic torques generate new counterrotating vortex pairs. Between $t = 15.75$ and $t = 18$, each secondary tongue is pinched off by a high pressure region and the recirculating part of one of the primary tongues, which splits again in this process into a layer leaving the vortex by its upper right and another that winds around along with the segmented secondary tongue. The process of formation of a secondary tongue and splitting of the recirculating flow occurs once again during this computation, and since there are several vortex pairs winding around, the vortex cores in Fig. 6b have for some time a multilayered structure until diffusion cancels vorticity of opposite signs (and temperature differences) leaving cores of predominantly negative vorticity ($t = 27$).

Finally these cores undergo a pairing, during which one or two more counterrotating vortex pairs are formed and ingested from the upper right of the forming vortex. At later times (not shown) these new pairs will become the front of a new tongue that heads toward the lower core moving toward the lower left while light fluid comes in behind and rolls around the surviving upper vortex. The result is an elongated structure with an associated decrease of E_1 in Fig. 4d.

Parts of the high temperature strip around the flame are alternatively strained and compressed by the evolving flow, and patches of fluid separate from this strip to form the tongues, but as was mentioned before, the flame itself remains outside

the vortex cores at least in the part of the evolution covered by these computations. This fact makes the flow in the vortices below the flame similar to a mixing layer between two fluids of different densities. To assess the extent of the similarity, further computations were carried out for an inert flow: $q = 0$ in the formulation of sec. 2 but $T_o = 5$, so that the maximum temperature of the fluid equals the flame temperature of the previous reacting flow simulation. Except for the absence of baroclinic vorticity production around the flame, the results of this simulation (not displayed) have the same general appearance as those of Fig. 6, though minor differences do occur.

Acknowledgments

We are indebted to Prof. A. Liñán for his continuous guide and advice and to Prof. J. Jiménez for enlightening discussions during the summer program.

REFERENCES

BROADWELL, J. E. & BREIDENTHAL, R. E. 1982 A simple model of mixing and chemical reaction in a turbulent shear layer. *J. Fluid Mech.* **125**, 397–410.

BROADWELL, J. E. & MUNGAL, M. G. 1991 Large-scale structures and molecular mixing. *Phys. Fluids A.* **3**, 1193–1206.

DELHAYE, B., VEYNANTE, D. & CANDEL, S. M. 1994 Simulation and modeling of reactive shear layers. *Theoret. Comput. Fluid Dynamics.* **6**, 67–87.

DIMOTAKIS, P.E. 1986 Two-dimensional shear-layer entrainment . *AIAA J.* **24**, 1791–1796.

DIMOTAKIS, P. E. 1991 Turbulent free shear layer mixing and combustion. In High-Speed Flight Propulsion Systems, Murthy, S. N. B., and Curran, E. T., eds, AIAA Inc.. *Progress in Astronautics and Aeronautics.* **137**, 265–340.

GHONIEM, A. F. & GIVI, P. 1988 Lagrangian simulation of a reacting mixing layer at low heat release. *AIAA J.* **26**, 690–697.

GIVI, P., JOU, W.-H. & METCALFE, R. W. 1986 Flame extinction in a temporally developing mixing layer. *Proc. 21nd. Int. Symp. Combustion.* The Combustion Institute, Pittsburgh. 1251–1261.

GRINSTEIN, F. F. & KAILASANATH, K. 1992 Chemical heat release and dynamics of transitional reactive shear flows. *Phys. Fluids A.* **4**, 2207–2221.

GOLDSTEIN, S. 1930 Concerning some solutions of the boundary layer equations in hydrodynamics. *Proc. Camb. Phil. Soc.* **26**, 1–30.

HERMANSON, J. C. & DIMOTAKIS, P. E. 1989 Effects of heat release in a turbulent, reactive shear layer. *J. Fluid Mech.* **199**, 333–375.

MARBLE, F. & BROADWELL, J. E. 1977 The coherent flame model for turbulent chemical reaction. Report No. TRW-9-PU. Project SQUID.

MASUTANI, S. M. & BOWMAN, C. T. 1986 The structure of a chemically reacting plane mixing layer. *J. Fluid Mech.* **172**, 93–126.

McMURTRY, P. A., JOU, W.-H., RILEY, J. J. & METCALFE, R. W. 1986 Direct numerical simulation of a reacting mixing layer with chemical heat release. *AIAA J.* **24**, 962–970.

McMURTRY, P. A., RILEY, J. J. & METCALFE, R. W. 1989 Effects of heat release on the large-scale structure in a turbulent mixing layer. *J. Fluid Mech.* **199**, 297–332.

MUNGAL, M. G. & DIMOTAKIS, P. E. 1984 Mixing and combustion with low heat release in a turbulent shear flow. *J. Fluid Mech.* **148**, 349–382.

MUNGAL, M. G. & FRIELER, C. E. 1988 The effects of Damkóhler number in a turbulent shear layer. *Comb. Flame.* **71**, 23–34.

MUNGAL, M. G., HERMANSON, J. C. & DIMOTAKIS, P. E. 1985 Reynolds number effects on mixing and combustion in a reacting shear layer. *AIAA J.* **23**, 1418–1423.

PLANCHÉ, O. H. & REYNOLDS, W. C. 1992 A numerical investigation of the compressible reacting mixing layer. Report TF-56. Dept. Mech. Engn. Stanford University, CA.

RILEY, J. J., METCALFE, R. W. & ORSZAG, S. A. 1986 Direct numerical simulations of chemically reacting turbulent mixing layers. *Phys. Fluids.* **29**, 406–422.

SHIN, D. S. & FERZIGER, J. H. 1991 Linear stability of the reacting mixing layer. *AIAA J.* **29**, 1634–1642.

WALLACE, A. K. 1981 Experimental investigation on the effects of chemical heat release in the reacting turbulent plane shear layer. Ph. D. Thesis. U. Adelaide.

WILLIAMS, F. A. 1985 *Combustion Theory,* 2nd ed. Benjamin/Cummings, Menlo Park CA.